PHILOSOPHICAL TRANSACTIONS OF THE ROYAL SOCIETY A MATHEMATICAL, PHYSICAL & ENGINEERING SCIENCES

High-Pressure Melting of Iron: New Experiments and Calculations

George Q. Chen and Thomas J. Ahrens

Phil. Trans. R. Soc. Lond. A 1996 **354**, 1251-1263
doi: 10.1098/rsta.1996.0047

High-pressure melting of iron: new experiments and calculations

By George Q. Chen and Thomas J. Ahrens

Lindhurst Laboratory of Experimental Geophysics, Seismological Laboratory, California Institute of Technology, Pasadena, CA 91125, USA

The melting curve of ϵ-iron in the pressure range of 100 GPa to 300 GPa has been derived by computing Gibbs free energies at high pressures and high temperatures from equation of states (EOS) of the α-, ϵ- and liquid phases. Our calculations indicate that the melting curve of iron is very sensitive to the EOS of both the solid (ϵ) and melt phases. Optimal EOS parameters for ϵ-iron are presented as well as new data for sound velocities in γ- and liquid phases. The latter provides a value for the Grüneisen parameter for liquid iron of 2.55 at 9.7 Mg m^{-3} at a pressure of 74 GPa.

Preliminary shock-wave experiments on pure iron preheated to 1300 °C were conducted in the 17–74 GPa range. Melting was observed in the highest pressure (74 GPa) experiment. This result supports our theoretically derived melting curve, which is close to those measured by Boehler (1993) and Saxena *et al.* (1993).

1. Introduction

The melting curve of ϵ-iron under high-pressure iron is directly related to the inner-core–outer-core temperature of the Earth. However, major disagreements exist between results from previous static (Williams *et al.* 1991; Boehler 1993; Saxena *et al.* 1993) and shock-wave measurements (Bass *et al.* 1987; Yoo *et al.* 1993). In this paper we attempt to theoretically determine the melting curve of iron from equation of states (EOS) of the α-, ϵ- and liquid phases in a thermodynamically consistent manner. The benefit of this approach can be twofold: (1) it is expected to yield results which demonstrate which of the previous high-pressure melting curves are consistent with available thermodynamic and EOS data; and (2) the calculations highlight thermodynamic quantities which need to be better determined in order to further constrain the melting curve.

The second part of this paper concentrates on preliminary shock-wave experiments on preheated iron samples. We determined the initial density shock-wave velocity and particle velocity in preheated (1300 °C) iron using the EOS methods pioneered by Miller *et al.* (1988). Using our velocity-interferometer-system-from-any-reflector (VISAR) system we also measured compressional-wave velocity in shock-compressed iron in the 17–74 GPa pressure range. The compressional-wave velocity provides an excellent diagnostic to detect melting under high pressures (Brown & McQueen 1986; Duffy & Ahren 1994*a*, *b*). Starting from the preshock temperature of 1300 °C, upon shock pressure of 74 GPa, sound velocities are measured which are comparable with that expected from interpolation between the high-pressure data of Brown & McQueen (1986), and 1 bar high-temperature sound velocity measurement on

Phil. Trans. R. Soc. Lond. A (1996) **354**, 1251–1263
Printed in Great Britain

Table 1. *Optimal EOS for α-, ϵ- and liquid iron*

phases	reference state[a]	EOS
α Huang *et al.* (1987)	$P_0 = 1$ bar, T_0=300 K $\rho_0 = 7.875$ g cm^{-3} $H_0 = 0$, $S_0 = 0$	$K_{T0} = 171$ GPa, $K'_{T0} = 4.0$ α and C_p data are after Robie *et al.* (1979), $\delta = 4.0$
ϵ (this paper)	$P_0 = 12$ GPa, T_0=300 K $\rho_0 = 8.775$ g cm^{-3} $H_0 = 8.144 \times 10^4$ J mol^{-1} $S_0 = -2.54$ J K^{-1} mol^{-1}	$K_{T0} = 205$ GPa, K'_{T0}=4.8, $\alpha_0 = 3 \times 10^{-5}$ K^{-1} $\beta = 2 \times 10^{-5}$, $\delta = 3.2$ $C_v = 0.9 \times (C_l + C_e)$
liquid Anderson & Ahrens (1994*a*)	$P_0 = 1$ bar, T_0=1809 K $\rho_0 = 7019$ kg m^{-3} $H_0 = 7.21 \times 10^4$ J mol^{-1} $S_0 = 72.3$ J K^{-1} mol^{-1}	$K_{S0} = 109.7$ GPa, K'_{S0}=4.661 $\gamma = 1.735 - 0.13 \times (\rho/\rho_0)^{-1.87} E$ $C_v = C_k + C_{pot} + C_e$[b]

[a] H_0, S_0 are relative to α-phase at 300 K, 1 bar.
[b] For exact forms of C_l, C_e, C_k and C_{pot} (see equation (2.13) and Anderson & Ahrens (1994)).

liquid iron (Nasch *et al.* 1994). In pressure–temperature (P–T) space the experiments conducted to date are compatible with our theoretically derived melting curve.

2. Gibbs free energy calculations

Two sets of equations are used in calculating Gibbs free energy (G) of a single phase as a function of P and T. These are discussed separately in later sections. The two methods are thermodynamically equivalent. The first method is more convenient for EOS given in terms of isothermal bulk modulus, K_{T0}, and its pressure derivative, K'_{T0} (e.g. assuming data for α- and ϵ-phases from static isothermal experiments). The second method employs an EOS given in terms of the equivalent isentropic parameters K_{S0} and K'_{S0} (liquid iron phase). Here the subscripts T and S indicate isothermal and isentropic conditions. The EOS of the three phases are listed in table 1.

(*a*) *Calculation using an isotherm–isobar mesh*

This approach was used by Song & Ahrens (1994) to evaluate the possibility of reactions between liquid iron in the outer core and silicates in lower mantle. In that paper, at any given pressure and temperature, Gibbs energies for the reactants and products were calculated and compared to determine the direction of reaction. Here we calculate and explicitly compare Gibbs energies of iron in different phases: the one that is lowest is the equilibrium phase under pressure P and temperature T. $G(P,T)$ is calculated from reference point $G(P_0,T_0)$ by first moving along the isobar to (P_0,T), then along the isotherm to the final state (P,T):

$$G(P,T) = H(P_0,T) - TS(P_0,T) + \int_{P_0}^{P} V(P',T)\,\mathrm{d}P' \qquad (2.1)$$

PHILOSOPHICAL TRANSACTIONS OF THE ROYAL SOCIETY A MATHEMATICAL, PHYSICAL & ENGINEERING SCIENCES

where the first two terms are

$$H(P_0,T) = H(P_0,T_0) + \int_{T_0}^{T} C_p(P_0,T')\,\mathrm{d}T', \tag{2.2}$$

$$S(P_0,T) = S(P_0,T_0) + \int_{T_0}^{T} \frac{C_p(P_0,T')}{T'}\,\mathrm{d}T', \tag{2.3}$$

$H(P_0,T_0)$ and $S(P_0,T_0)$ are enthalpy and entropy of formation from elements, V and C_p are volume and specific heat at constant pressure.

For the last term on the right-hand side of equation (2.1), $V(T,P')$ is again calculated on the P'–T mesh: First, $V(T_0,P')$ is calculated from, for example, third-order Birch–Murnaghan EOS

$$P' = \tfrac{3}{2}K_{T0}\left\{\left[\frac{V(P_0,T_0)}{V(P',T_0)}\right]^{7/3} - \left[\frac{V(P_0,T_0)}{V(P',T_0)}\right]^{5/3}\right\} \times(1+\tfrac{3}{4})(K'_{T0}-4)\left[\left(\frac{V(P_0,T_0)}{V(P',T_0)}\right)^{2/3} - 1\right] \tag{2.4}$$

given the volume, isothermal bulk modulus K_{T0} and its derivative K'_{T0} at the reference state (table 1). Then it undergoes thermal expansion to the final state:

$$V(P',T) = V(P',T_0)\exp\left[\int_{T_0}^{T}\alpha(P',T')\,\mathrm{d}T'\right] \tag{2.5}$$

The thermal expansion coefficient $\alpha(P',T')$ is usually experimentally determined only at $P' = 1$ bar. The pressure dependence assumed is

$$\alpha(P',T') = \alpha(P_0,T')\left[\frac{V(P',T')}{V(P_0,T')}\right]^{\delta}, \tag{2.6}$$

where δ is the second Grüneisen parameter, which is taken to be constant (see table 1 for values).

Gibbs energies of the α- and ϵ-phases of iron are calculated with this method.

The calculation is carried out numerically on a $N_P \times N_T$ mesh in the P–T space: $P_i = P_0 + i \times \Delta P$, $T_j = T_0 + j \times \Delta T$ (i, j are indices of nodes). Evaluating equations (2.1)–(2.5) numerically is fairly straightforward; for equation (2.6), one needs to know $V(P' = P_i, T' = T_j)$, which requires $\alpha(P' = P_i, T' = T_j)$ to be known beforehand. Although the problem may be solved by iteration (together with equation (2.5)), we use an approximate solution for $\alpha(P',T')$ from $V(P_{i-1},T_j)$ (which has been calculated at this point):

$$\alpha(P_i,T_j) = \alpha(P_0,T_j)\left[\frac{V(P_{i-1},T_j)}{V(P_0,T_j)}\right]^{\delta}. \tag{2.7}$$

(*b*) *Calculation using an isentrope–isometric mesh*

The calculation of the Gibbs energy of liquid iron employs

$$G(P,T) = E(P,T) - TS(P,T) + PV(P,T). \tag{2.8}$$

At any P and T, E, S and V are calculated by first moving along an isentrope

from (P_0, T_0) to (P_S, T_S), at which the internal energy is E_S and volume is $V_S(= V)$:

$$E_S(P_S) = E(P_0, T_0) - \int_{V_0}^{V_S} P_S \, \mathrm{d}V, \tag{2.9}$$

$$T_S(P_S) = T_0 \exp\left[- \int_{V_0}^{V_S} \left(\frac{\gamma}{V}\right) \mathrm{d}V \right], \tag{2.10}$$

where V_S is again determined by third-order Birch-Murnaghan EOS (same as equation (2.4), except that K_{T0} and K'_{T0} in the equation are replaced with isentropic bulk modulus K_{S0} and its pressure derivative K'_{S0}). γ is the Grüneisen parameter; for liquid iron, it has been fit as a function of internal energy, i.e. in equation (2.10), $\gamma = \gamma(E_S)$. The integral can then be evaluated, noting along the isentrope that $\mathrm{d}E_S = -P_S \, \mathrm{d}V$.

The second step is to move along an isovolumetric line from (P_S, T_S) to (P, T). With $V(P, T)$ held at constant V_S, either P or T are variable. We treat the isentropic pressure P_S and final pressure P as dependent parameters; therefore, $T = T(P, P_S)$. The internal energy of the final state (E) is given by solving the Mie–Grüneisen equation:

$$\int_{E_S}^{E} \gamma(E') \, \mathrm{d}E' = V_S(P - P_S), \tag{2.11}$$

then the following equation is solved for T:

$$\int_{T_S}^{T} C_v(T', V_S) \, \mathrm{d}T' = E - E_S, \tag{2.12}$$

and S is

$$S = S_0 + \int_{T_S}^{T} \frac{C_v(T', V_S)}{T'} \, \mathrm{d}T'. \tag{2.13}$$

Equations (2.11)–(2.13) give all the thermodynamic quantities needed to evaluate equation (2.8), given values for K_{S0}, K'_{S0}, C_v and γ.

(*c*) *Gibbs energy of α- and liquid iron*

Huang *et al.* (1987) reported α-iron high-pressure compression data to 12.4 GPa with a reference state at 1 bar and 300 K. We used the experimental α-iron C_p data of Robie *et al.* (1979) (alternatively one can estimate theoretically by summing lattice, magnetic and electronic contributions (Kerley 1993)).

For liquid iron, the reference state is at the melting point (1809 K) at 1 bar. H_0 and S_0 are calculated from the values of the α-phase at the same pressure and temperature, and the enthalpy change upon melting. We used the EOS parameters of liquid iron in Anderson & Ahrens (1994) (table 1). This EOS was obtained based on data from a wide range of experiments: ultrasonic, thermal expansion and enthalpy data at 1 bar, pulse heating, shock-wave compression and sound velocity from STP to 10^3 GPa and 8000 K.

(*d*) *Gibbs energy of ϵ-iron*

K_{T0} and K'_{T0} for ϵ-iron are obtained from analysis of X-ray diffraction under static compression (Huang *et al.* 1987; Mao *et al.* 1990). Thermal expansion coefficient is poorly constrained, previous estimates from static experiments exist in the 150–450 °C, 10–20 GPa region (*ca.* 3–5×10^{-5} K^{-1} (Huang *et al.* 1987)), shock-wave data

yield a mean value of α from 300 to *ca.* 5200 K at 202 GPa ($\sim 9\times10^{-6}$ K^{-1} (Duffy & Ahrens 1993). No experimental data is available for the specific heat. We calculated C_v by summing the contributions from the lattice (given by the Debye model) and from the electrons. For the electronic contribution (C_e), we adopted the theoretical results of Boness *et al.* (1986). We assumed the following value for C_v:

$$C_v(P,T) = c\left[9R\times D\left(\frac{T_D}{T}\right) + C_\mathrm{e}\right], \tag{2.14}$$

where D is the Debye function, and Debye temperature for ϵ-iron is 385 K (Andrews 1973; Kerley 1993). Here c is an *ad hoc* parameter: if our model is correct, c is unity.

C_p is then calculated from C_v from the thermodynamic identity

$$C_p = C_v + \alpha^2 V K_{T0} T. \tag{2.15}$$

The reference state is chosen to be (12 GPa, 300 K), at which the α-phase transforms to the ϵ-phase. The entropy change of the transition, ΔS, at 300 K is unknown, but from the Clausius–Claperon relation

$$\Delta S = \Delta V \frac{\mathrm{d}P}{\mathrm{d}T}, \tag{2.16}$$

(ΔV is the volume change during the α–γ phase change at 300 K (Huang *et al.* 1987) and $\mathrm{d}P/\mathrm{d}T$ is the slope of the phase boundary in the P–T plane (reviewed in Besson & Nicol 1990); it is estimated the enthalpy change $\Delta H = T\Delta S$ is no more than *ca.* 0.6 kJ mol^{-1}, or about 5% of the enthalpy increase of iron upon melting under 1 bar. In absence of more accurate data, we set ΔH to zero in our calculations.

(*e*) *Melting curve between the ϵ- and liquid phases*

After the Gibbs energies of the ϵ- and liquid-phases (G_ϵ and G_l) are calculated independently, the melting temperature is defined as the intersection of the two curves of Gibbs energy versus temperature at constant pressure. We keep the α- and liquid-phases EOS fixed and adjust the ϵ-phase EOS to fit experimentally determined melting curves (Boehler 93; Williams *et al.* 1991; Saxena *et al.* 1994). The results are shown in figure 1.

In the following sections we discuss the effects of various parameters (C_p, K_{T0}, α) of the ϵ-phase which are not well determined from experiments.

(i) *Specific heat*

We vary C_p by changing the parameter c in equation (2.14). It has a pronounced effect on the slope of the $G_\epsilon(T)$ at a given pressure. The effect is nearly the same at different pressures. At $c = 1$ (the theoretical value), $G_\epsilon(T)$ drops faster than $G_\mathrm{l}(T)$ at higher pressures (200–300 GPa) such that they may never intersect. This is in clear contradiction with experimental data. The deviation of c from unity indicates large anharmonicity in the close-packed ϵ-phase or uncertainty in determination of the electronic specific heat.

(ii) *Bulk modulus*

The bulk modulus controls the slope of $G_\epsilon(P)$ versus P at a given temperature. The effect decreases with increasing T due to the K_{T0} temperature dependence, so K_{T0} also affects the slope of $G_\epsilon(T)$, though much less directly than C_p does. The effect can further be refined by varying K'_{T0}.

PHILOSOPHICAL TRANSACTIONS OF THE ROYAL SOCIETY A MATHEMATICAL, PHYSICAL & ENGINEERING SCIENCES

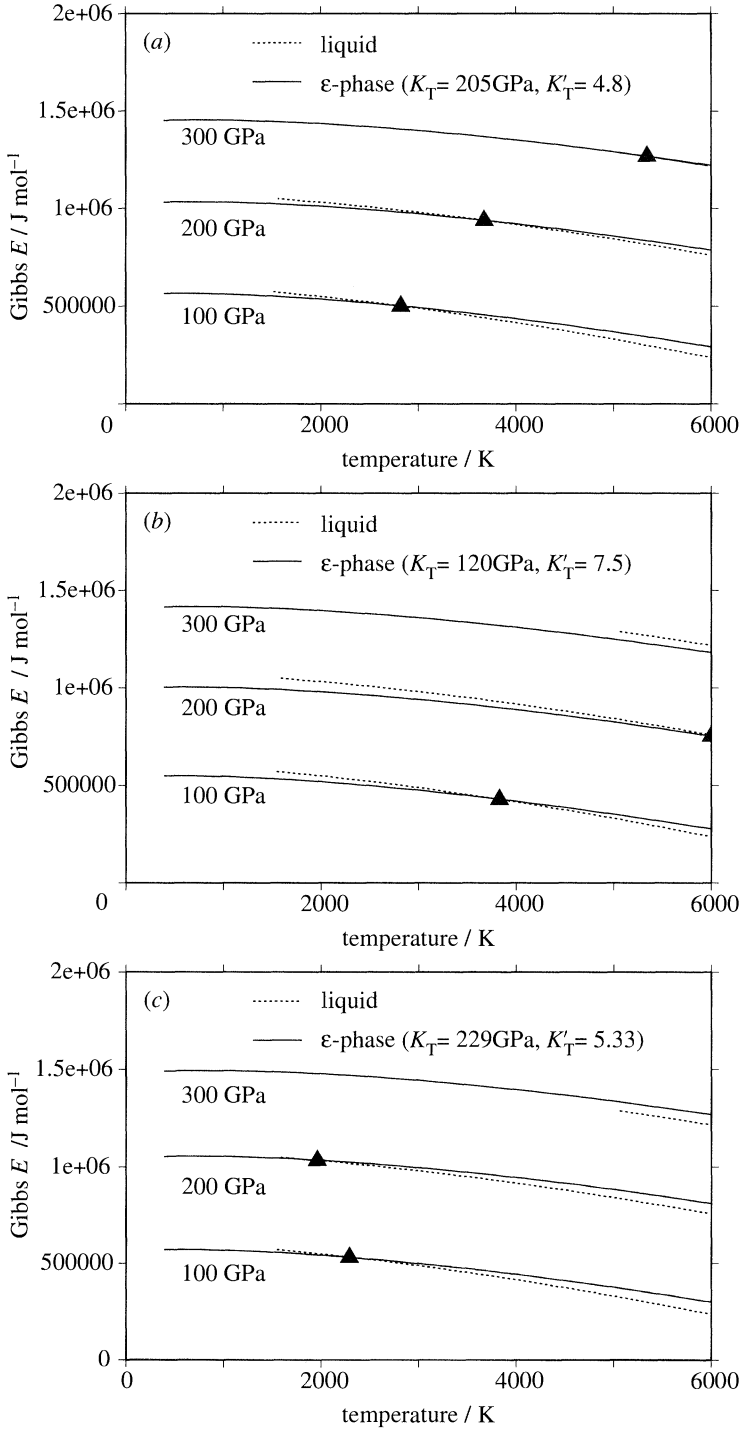

Figure 1. Gibbs free energies of the ϵ- and liquid iron as functions of pressure. Their intersections (melting points) change as we use the three sets of EOS parameters in table 1 for ϵ-iron: (*a*) intersections are close to Boehler's (1993) melting curve; (*b*) intersections close to Williams *et al.*'s (1991) melting curve; (*c*) intersections obtained with Mao *et al.*'s (1990) experimental data.

PHILOSOPHICAL TRANSACTIONS OF THE ROYAL SOCIETY A MATHEMATICAL, PHYSICAL & ENGINEERING SCIENCES

(iii) *Thermal expansion*

α has a similar effect on $G_\epsilon(P)$ at fixed pressures as C_p (lower values of α give steeper $G_\epsilon(P)$ versus T curves), but the change of slope has much stronger pressure dependence than that caused by C_p. Again, the effect can be subtly controlled with the temperature dependence of α ($1/\alpha_0(\partial\alpha/\partial T)_p \equiv \beta$) and its pressure dependence as specified by equation (2.6).

3. *P–T* phase diagrams of iron

The diamond-anvil melting curves (Boehler 1993; Saxena *et al.* 1993) agree closely regarding the solid–liquid stability field (although they disagree about the stability region of a proposed new β-phase, see figure 2). Saxena *et al.* (1994) proposed the phase diagram shown in figure 2 based on their experimental data and thermodynamic calculations similar to ours. Yoo *et al.*'s (1993) shock-wave data agree with a melting curve proposed earlier in Williams *et al.*'s (1991) review of static compression and Bass *et al.*'s (1987) Hugomiot temperature data. Recently, Anderson & Ahrens (1996) revised shock temperature calculations of Bass *et al.* (1987), which derived a lower melting point at high pressures (greater than 230 GPa), but not low enough to explain the difference between the (low-pressure) static melting curves and Bass *et al.*'s (1987) (high-pressure) shock-wave data. The origin of the solid–solid transformation observed in the principal Hugoniot (at *ca.* 200 GPa (Brown & McQueen 1986)) before melting (at *ca.* 243 GPa) is uncertain. Brown & McQueen (1986) interpreted it as the ϵ–γ transition (figure 4), while Boehler (1993) believed it to be between ϵ and β. Anderson (1994) offered a third scenario by suggesting yet another solid phase θ above 200 GPa and 4000 K. Structure studies of the β-phase are only theoretical. Matsui (1992) suggested that it should have a body centred cubic (BCC) structure from his molecular simulations, but Stixrude & Cohen (1995) concluded that BCC structure is unstable in the *ca.* 150 GPa range from density functional theory. It is likely that there is at least one phase between the ϵ and liquid stability fields in the pressure range of 100–300 GPa, but the EOS of the phase is unknown and hence calculating its fusion curve is infeasible.

Our best estimate of the ϵ-liquid-phase line calculated from thermodynamic and EOS data (table 1) is given in figure 2.

4. Preheated shock-wave experiments

Five shock-wave experiments have been conducted on the 40 mm propellant gun at Caltech in the 17–74 GPa range (table 2). The pure iron targets are in the form of discs, flat on one side, and stepped on the other, the central thickness is *ca.* 6 mm, while the driver plate is about 2 mm thick. The target is heated via a induction coil on the top hat side before it is impacted on the flat side. The temperature is monitored until just before impact with a two-colour infrared pyrometer (Williamson 8120S-C-WD2) which in turn was calibrated against a thermocouple. The variation in temperature in target is estimated to be about $\pm 30\,^\circ$C at preshock temperature $1300\,^\circ$C. The five experiments are of two types: EOS and VISAR (figure 3). A detailed description of the two types can be found in Miller *et al.* (1988) and Duffy & Ahrens (1994*b*), respectively. In short, the first type monitors optical reflectivity on the (stepped) back surface of the target which decreases rapidly upon shock arrival.

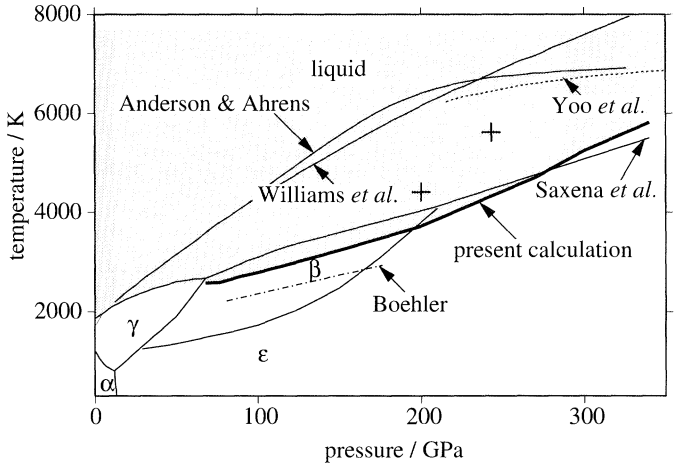

Figure 2. Present calculated melting curve in comparison to previously suggested phase diagrams. Boehler's (1993) and Saxena *et al.*'s (1993) melting curves are very close, which are plotted and labelled collectively as 'Saxena *et al.*'. The chain line labelled 'Boehler' is his β–ϵ boundary. The melting curves from shock-wave data are all higher than static curves. The two crosses at 200 and 243 GPa are calculated shock temperatures of solid–solid transition and melting along the principal Hugoniot of Brown & McQueen (1986).

Table 2. *High-temperature EOS and VISAR shock-wave experiments on iron*

shot (type)	flyer plate	impact velocity (km s^{-1})	pressure (GPa)	density (g cm^{-3})	sound velocity (km s^{-1})
946 (EOS)	Al	1.432	17.4	8.246	
961 (VISAR)					6.38
944 (EOS)	Ta	1.574	41.4	8.957	
945 (EOS)	Ta	2.513	74.4	9.733	
959 (VISAR)					6.52

In experiments we measure initial density (via the measurement of initial temperature), shock-wave velocity and projectile velocity, and derive particle velocity, shock pressure and the high-pressure specific volume. The VISAR experiments use a modified Michaelson interferometer to measure the Doppler shift of a laser beam reflected from the back surface of the moving target. In our experiments the free-surface of the iron target first accelerates upon shock arrival, then decelerates when the release wave from the back of the flyer plate has propagated to the free-surface. The initial release velocity (which equals to compressional sound velocity in solids and bulk sound velocity in liquids) in pressurized iron can be calculated from the time interval between the acceleration and deceleration of the free-surface. The arrangement is modified from Duffy & Ahrens (1994*b*) for the high-temperature environment of our experiments, but the basic principle is unchanged. Four of the five experiments are paired at nearly the same shock conditions.

PHILOSOPHICAL TRANSACTIONS OF THE ROYAL SOCIETY A MATHEMATICAL, PHYSICAL & ENGINEERING SCIENCES

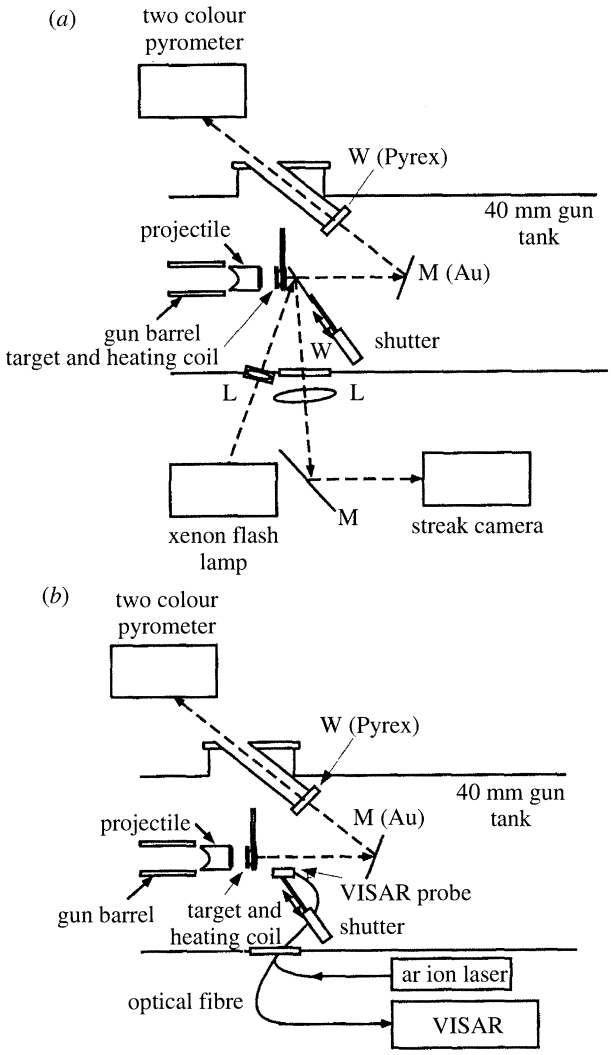

Figure 3. Experimental assemblies for (*a*) EOS and (*b*) VISAR experiments. The iron target is preheated with RF induction coils and its temperature is monitored by the pyrometer. Moments before launching the projectile, the EOS turning mirror or the VISAR probe is inserted in front of the target free-surface.

(*a*) *Phase determination*

The 1300 °C Hugoniot in pressure–volume space is shown in figure 4 together with the principal Hugoniot. The high-temperature Hugoniot obtained so far (up to 74 GPa) is shifted from the principal Hugoniot by a nearly constant factor (thermal expansion at 1 bar, which is about 5.7%). As the solid–liquid transition is not prominent in the P–V space, the EOS experiments are not adequate for detecting melting.

The initial release velocity data are plotted in figure 5 as a function of shock pressure. Also plotted in the figure are previous measurements by Brown & McQueen (1986) and Nasch *et al.* (1994) for ϵ-, γ- and liquid iron. It can be seen that our 74 GPa datum agrees very well with liquid iron data, while the 17 GPa datum

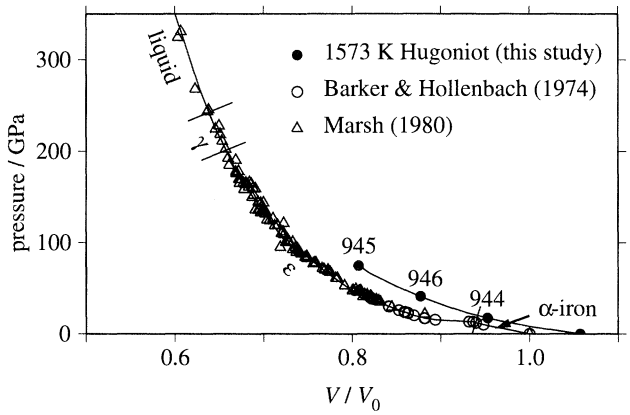

Figure 4. High-temperature (1300 °C) Hugoniot of this study compared to the principal Hugoniot. Specific volume is normalized to that of iron at STP V_0.

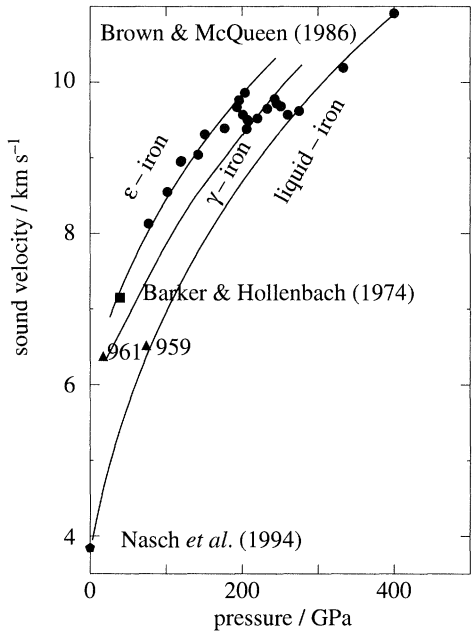

Figure 5. Sound velocity data of this study and those of previous studies.

lies approximately on the γ-iron curve. We conclude iron is molten in the 74 GPa experiment.

In figure 6 we plot the shock temperatures in reference to the different melting curves. The shock temperature achieved in shot 945 is calculated at its shock pressure and volume using the complete EOS of liquid iron from Anderson & Ahrens (1994*a*). Shock temperatures of 944 and 946 given by the same EOS are too low to be in the liquid-phase and are recalculated assuming that they are in the γ-phase. The method used is to equate the shock-wave-induced internal energy increase to the sum of isotherm compression energy and energy of heating at constant volume:

$$E = \tfrac{1}{2}P(V - V_0) = -\int_{V_0}^{V} P_{T_0}\,\mathrm{d}V + \int_{T_0}^{T} C_V\,\mathrm{d}T. \tag{4.1}$$

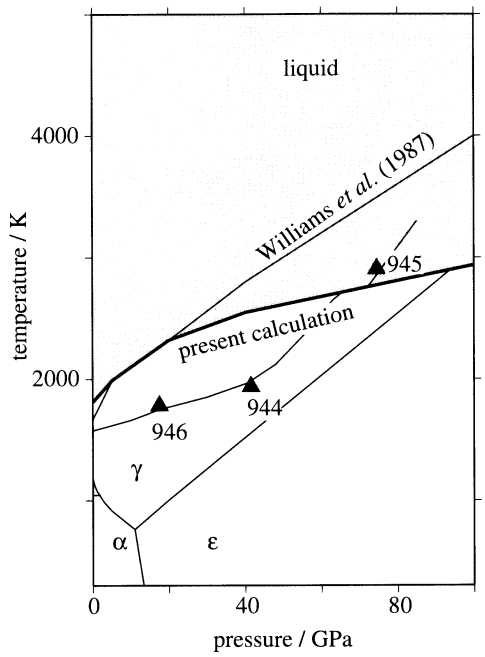

Figure 6. Shock temperatures of the experiments in table 2 and their relation to different melting curves.

The first term is calculated with the Murnaghan equation, with $K_{T0} = 127$ GPa and $K'_{T0} = 2.2$ (Boehler *et al.* 1989). C_V is $3R$ in the second term.

Our sound velocity measurements and the conclusion that iron is in the liquid field at 74 GPa are compatible with the theoretical melting line of table 1 and figure 2.

(*b*) *Grüneisen parameters of the liquid and γ-phases*

Assuming a linear relation between shock-wave velocity U_s and particle velocity u_p,

$$U_s = c_0 + s u_p. \tag{4.2}$$

c_0 and s are determined from our EOS experiments to be 4116.3 m s^{-1} and 1.57. The Grüneisen parameter γ for liquid iron can be calculated from the bulk sound velocity V_b using the following equation:

$$\gamma = \frac{\rho_0[1 + s\eta + R^{*2}(s\eta - 1)]}{\rho s \eta^2}, \tag{4.3}$$

where $\eta = u_p/U_s$, $R^* = \rho V_b/(\rho_0 U_s)$ (Anderson & Ahrens 1994*a*). Our V_b of 6520 m s^{-1} gives $\gamma = 2.55$ at $\rho = 9.733$ g cm^{-3}, which is higher than the data of Brown & McQueen (1986) at *ca.* 1.5 for ρ between 12 and 14 g cm^{-3}.

Since the longitudinal sound velocity V_p is measured for the solid γ-phase, the above equation cannot be used until the Poisson's ratio ν is known and V_b can be derived from V_p:

$$V_b = V_p \sqrt{\frac{1+\nu}{3(1-\nu)}}. \tag{4.4}$$

Poisson's ratio is strongly dependent on pressure and has been modelled in Falzone

& Stacey (1980). However, we found that the value of γ varies drastically with small changes in ν. Therefore, determination of the γ-phase Grüneisen parameter is not attempted.

5. Conclusions

Current revisions of earlier shock temperature measurements involving thermal diffusivity corrections (Gallagher *et al.*, personal communication) appear to move these temperatures down to good agreement with the earlier Brown & McQueen (1986) calculations. The ϵ-liquid melting curve of iron presented in figure 2 is in good agreement with the data of Boehler (1993) and Saxena *et al.* (1994). The value of K_{T0} of ϵ-iron at 12 GPa and 300 K which will give a melting line in exact agreement with the data of Boehler (1993) is 205 GPa (table 1), significantly lower than the 264 GPa (with $K'_{T0} = 5$) reported by Huang *et al.* (1987). The 205 GPa bulk modulus value is closer to 229 GPa, which was measured by Mao *et al.* (1990). Mao's data, however, yields a melting curve too low in the 100–300 GPa range (figure 1*c*). Interestingly, values of $K_{T0} \simeq 120$ GPa and $K'_{T0} = 7.5$ for ϵ-iron are required to fit the data of Williams *et al.* (1991). Therefore, assuming the phase diagram and the EOS of the α- and liquid phases are approximately correct, our calculations favour Saxena *et al.* (1994) and Boehler's (1993) melting curve over that of Williams *et al.* (1991). Finally, in either fit, the specific heat of the ϵ-phase is 10% lower than the theoretical value derived by Boness *et al.* (1986) ($c = 0.90$ in equation (2.14)).

Although we cannot completely delineate the effects of all variables on the Gibbs energy of the ϵ-phase, we note that to fit the data of Williams *et al.* (1991), the bulk modulus must be lowered to fit the melting point at 100 GPa (*ca.* 4000 K). Although steepening the Gibbs energy temperature dependence (by, for example, increasing the value of C_p) would also raise the melting point at 100 GPa; it yields too high a melting point at 200 GPa. More experimental data on the β- and ϵ-phases (especially to better define the existence of the β-phase and to determine the ϵ-phase's thermal expansion coefficient) would lead to more definite conclusions from our calculations.

Preheated EOS and VISAR experiments are proven to be valuable techniques to obtain absolute values of sound velocities in the γ- and liquid phases and, hence, the Grüneisen parameter for the liquid phase at 74 GPa of 2.55. In agreement with the Gibbs energy calculations, our preliminary experimental results strongly supports Saxena *et al.* (1994) and Boehler's (1993) melting curve.

Research supported by NSF. We thank William Anderson for helpful discussions, Wenbo Yang, Mike Long and E. Gelle's assistance in the experiments and Andrew Jephcoat and two anonymous referees for helpful comments. Contribution # 5524, Division of Geological and Planetary Sciences, California Institute of Technology.

References

Anderson, O. L. 1994 Imperfections of the 1993 phase diagram of iron. In *High pressure science and technology—1993* (ed. S. C. Schmidt, J. W. Shaner, G. A. Samara & M. Ross) pp. 907–910. New York: American Institute of Physics Press.

Anderson, W. W. & Ahrens, T. J. 1994 An equation of state for liquid iron and implications for the Earth's core. *J. Geophys. Res.* **99**, 4273–4284.

Anderson, W. W. & Ahrens, T. J. 1996 Shock temperatures and melting in iron sulfides at core pressures. *J. Geophys. Res.* (In the press.)

Andrews, D. J. 1973 Equation of state of the alpha and epsilon phases of iron. *J. Phys. Chem. Solids* **34**, 825–840.

Bass, J. D., Svendsen, B. & Ahrens, T. J. 1987 The temperatures of shock-compressed iron. In *High pressure research in mineral physics* (ed. M. Manghnani & Y. Syono), pp. 393–402. Tokyo: Terra.

Besson, J. M. & Nicol, M. 1990 An equation of state of γ-Fe and some insights about magnetoelastic effects on measurements of the α–γ–ϵ triple point and other transitions. *J. Geophys. Res.* **95**, 21 717–21 720.

Boehler, R. 1993 Temperatures in the Earth's core from melting-point measurements of iron at high static pressures. *Nature* **363**, 534–536.

Boehler, R., Besson, J. M., Nicol, M., Nielsen, M., Itie, J. P., Weill, G., Johnson, S. & Grey, F. 1989 X-ray diffraction of γ-iron at high temperatures and pressures *J. Appl. Phys.* **65**, 1795–1797.

Boness, D. A., Brown, J. M. & McMahan, A. K. 1986 The electronic thermodynamics of iron under Earth core conditions. *Phys. Earth Planet. Inter.* **42**, 227–240.

Brown, J. M. & McQueen, R. G. 1986 Phase transitions, Grüneisen parameter, and elasticity for shocked iron between 77 GPa and 400 GPa. *J. Geophys. Res.* **91**, 7485–7494.

Duffy, T. S. & Ahrens, T. J. 1994*a* The temperature sensitivity of elastic-wave velocity at high-pressure—New results for molybdenum. *Geophys. Res. Lett.* **21**, 473–476.

Duffy, T. S. & Ahrens, T. J. 1994*b* Dynamic-response of molybdenum shock-compressed at 1400 °C. *J. Appl. Phys.* **76**, 835–842.

Falzone, A. J. & Stacey, F. D. 1980 Second-order elasticity theory: explanation for the high Poisson's ratio of the inner core. *Phys. Earth Planet. Inter.* **21**, 371–377.

Huang, E., Bassett, W. A. & Tao, P. 1987 Pressure–temperature–volume relationship for hexagonal close packed iron determined by synchrotron radiation. *J. Geophys. Res.* **92**, 8129–8135.

Kerley, G. I. 1993 Multiphase equation of state for iron. Sandia report, SAND93-0027.

Mao, H. K., Wu, Y., Chen, L. C., Shu, J. F. & Jephcoat, A. P. 1990 Static compression of iron to 300 GPa and $Fe_{0.8}Ni_{0.2}$ alloy to 260 GPa: implications for composition of the core. *J. Geophys. Res.* **95**, 21 737–21 742.

Matsui, M. 1992 Computer simulation of the structural and physical properties of iron under ultra high pressures and high temperatures. *Central Core Earth* **2**, 79–82.

Miller, G. H., Ahrens, T. J. & Stolper, E. M. 1988 The equation of state of molybdenum at 1400 °C. *J. Appl. Phys.* **63**, 4469–4475.

Nasch, P. M., Manghnani, M. H. & Secco, R. A. 1994 Sound-velocity measurements in liquid-iron by ultrasonic interferometry. *J. Geophys. Res.* **99**, 4285–4291.

Robie, R. A., Hemingway, B. S. & Fisher, J. R. 1979 Thermodynamic properties of minerals and related substances st 298.15 K and 1 bar (10^5 Pascals) pressure and at higher temperatures. *U.S. Geol. Surv. Bull.* 1452.

Saxena, S. K., Shen, G. & Lazor, P. 1993 Experimental evidence for a new iron phase and implications for Earth's core. *Science* **260**, 1312–1314.

Saxena, S. K., Shen, G. & Lazor, P. 1994 Temperatures in Earth's core based on melting and phase transformation experiments on iron. *Science* **264**, 405–407.

Song, X. & Ahrens, T. J. 1994 Pressure–temperature range of reactions between liquid iron in the outer core and mantle silicates. *Geophys. Res. Lett.* **21**, 153–156.

Stixrude, L. & Cohen, R. E. 1995 Constraints on the crystalline structure of the inner core: mechanical instability of BCC iron at high pressure. *Geophys. Res. Lett.* **22**, 125–128.

Williams, Q., Knittle, E. & Jeanloz, R. 1991 The high-pressure melting curve of iron—a technical discussion. *J. Geophys. Res.* **96**, 2171–2181.

Yoo, C. S., Holmes, N. C., Ross, M., Webb, D. J. & Pike, C. 1993 Shock temperatures and melting of iron at Earth core conditions. *Phys. Rev. Lett.* **70**, 3931–3934.

PHILOSOPHICAL TRANSACTIONS OF THE ROYAL SOCIETY A MATHEMATICAL, PHYSICAL & ENGINEERING SCIENCES